Deep-Sea Research I 65 (2012) 46–58

Contents lists available at SciVerse ScienceDirect

Deep-Sea Research I

journal homepage: www.elsevier.com/locate/dsri

On the surface circulation of the Levantine sub-basin derived from Lagrangian drifters and satellite altimetry data

Milena Menna [a,*], Pierre-Marie Poulain [a], George Zodiatis [b], Isaac Gertman [c]

[a] Istituto di Oceanografia e Geofisica Sperimentale—OGS, Sgonico (TS), Italy
[b] Oceanography Center, University of Cyprus, Nicosia, Cyprus
[c] Israel Oceanographic and Limnological Research, Haifa, Israel

ARTICLE INFO

Article history:
Received 7 November 2011
Received in revised form
21 February 2012
Accepted 28 February 2012
Available online 7 March 2012

Keywords:
Levantine sub-basin
Drifter data
Sea level anomaly
Geostrophic currents
Seasonal statistics
Eddy variability

ABSTRACT

The surface currents of the Levantine sub-basin (Mediterranean Sea) are described using 18 years (1992–2010) of drifter data and satellite-derived sea level anomalies. The combination of drifter and satellite data allowed to estimate maps of surface geostrophic circulation and to obtain more accurate pseudo-Eulerian velocity statistics for different time periods. Seasonal and interannual variability of surface currents are investigated with particular focus on the main sub-basin eddies of the eastern Levantine. The mean velocity field depicts the typical patterns of the along-slope and offshore currents and outlines the sub-regions where eddies are generated recurrently (west Egyptian coast, Ierapetra, Mersa-Matruh, south-west of Cyprus, Israel–Lebanon coast, Latakia) or persist steadily (Rhodes Gyre). Highly variable and energetic currents are observed between the Ierapetra and Mersa-Matruh regions, as the result of the interaction of the Mid-Mediterranean Jet meandering in between, and interacting with, the eddies generated by the instability of the coastal current. Seasonal pseudo-Eulerian maps show the current field stronger in summer and weaker in winter, mainly in the western Levantine and in the Cyprus–Syria Passage. The Shikmona Eddy displays a periodic nature with higher intensities during the cold months and an enhanced activity in the period 1998–2005. The Cyprus Eddy has a less periodic nature, characterised by events of high activity and periods in which it dominates as a single enlarged eddy in the southeast Levantine, eventually including the Shikmona Eddy. The Latakia Eddy is mainly cyclonic with higher intensities in summer and fall; occasional weekly or monthly inversions of circulation from cyclonic to anticyclonic are triggered by the interaction between the MMJ and the northward coastal meandering current.

1. Introduction

Even though the investigation of the Eastern Mediterranean Sea (EMS; see Table 1 for a list of acronyms used in this paper) was started almost hundred years ago (the first circulation scheme was proposed by Nielsen in 1912), many aspects of the circulation, in particular in the Levantine sub-basin (LSB), are still open or under debate. The older circulation schemes (Nielsen, 1912; Ovchinnikov, 1966; Ovchinnikov et al., 1976; Robinson et al., 1991; Özsoy et al., 1993; Robinson and Golnaraghi, 1993; Malanotte-Rizzoli et al., 1997), derived from hydrographic data, provided the basin scale characteristics of the EMS. More recently, studies carried out using satellite time series of sea surface temperature (SST) (Hamad et al., 2006; Millot and Taupier-Letage, 2005), sea surface height (SSH) and sea level anomaly (SLA) (Ayoub et al., 1998; Larnicol et al., 2002; Pascual et al., 2007; Rio et al., 2007; Amitai et al., 2010), numerical model simulations (Tziperman and Malanotte-Rizzoli, 1991; Lascaratos et al., 1993; Pinardi and Masetti, 2000; Alhammoud et al., 2005; Pinardi et al., 2006) and satellite-tracked drifters (Gerin et al., 2009), revealed ubiquitous sub-basin and mesoscale circulation patterns.

The easternmost part of the EMS, known as LSB and defined in this paper as the area between 25°E and 36°E (see Fig. 1 for geographical references), was studied extensively in the last years to solve some doubts concerning its complicated surface circulation. A short summary of the LSB oceanographic characteristics follows hereafter. On basin scale, the LSB circulation is characterised by an along-slope anticlockwise current, composed of an eastward branch to the south, named the Libyo-Egyptian Current (LEC) (Millot and Taupier-Letage, 2005; Gerin et al., 2009; Millot and Gerin, 2010), and of a westward branch to the north, called Asia Minor Current (AMC) (Özsoy et al., 1991; Robinson et al., 1991; POEM Group, 1992; Zodiatis et al., 2005). Robinson et al. (1991, 2001) as well as Pinardi et al. (2006), Zodiatis et al. (2010) and Pinardi et al. (2011) suggested also the existence of

* Correspondence to: OGS, Borgo Grotta Gigante, 42/c, 34010 Sgonico (TS), Italy. Tel.: +39 03383019108; fax: +39 040327307.
E-mail address: mmenna@ogs.trieste.it (M. Menna).

0967-0637/$ - see front matter © 2012 Elsevier Ltd. All rights reserved.
doi:10.1016/j.dsr.2012.02.008

Table 1
List of the acronyms used in this paper.

Geographical names	
EMS	Eastern Mediterranean Sea
LSB	Levantine sub-basin
Physical properties	
ADT	Absolute Dynamic Topography
AGV	Absolute Geostrophic Velocity
EKE	Eddy Kinetic Energy
KE	Kinetic Energy of velocity residuals
MKE	Mean Kinetic Energy
SLA	Sea Level Anomaly
SMDT	Synthetic Mean Dynamic Topography
SSH	Sea Surface Height
SST	Sea Surface Temperature
Currents	
AMC	Asia Minor Current
CC	Cilician Current
LEC	Libyo-Egyptian Current
MMJ	Mid-Mediterranean jet
Gyres and Eddies	
CE	Cyprus Eddy
EE	Egyptian eddies
IE	Ierapetra Eddy
LTE	Latakia Eddy
MME	Mersa-Matruh Eddy
RG	Rhodes Gyre
ShE	Shikmona Eddy

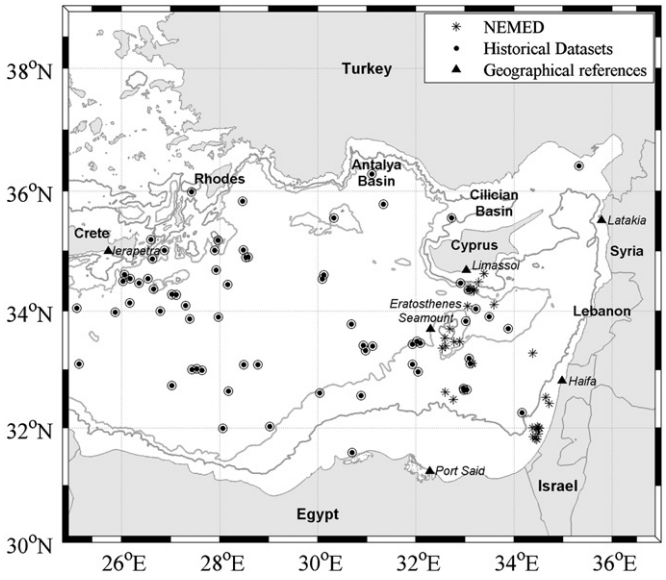

Fig. 1. Geography and bathymetry of the Levantine sub-basin. Asterisks show the sites of NEMED drifter deployments; black circles show the sites of historical drifter deployments. The 1000 m and 2000 m isobaths are shown with light grey lines.

a central eastward cross-basin meandering current named Mid-Mediterranean Jet (MMJ), that flows from ~24°E to southeast of Cyprus and which can lead to the generation of mesoscale features. At sub-basin scale, the LSB circulation is dominated by gyres and eddies, that can be forced by the wind or controlled by bathymetry or generated by instability of the along-slope and offshore currents. The north-western part of LSB is dominated by the persistent cyclonic Rhodes Gyre (RG; diameter of about 300 km), located southwest of Turkey and east of Rhodes Island, and depicted by some authors as the result of interaction of the wind driven basin circulation with the MMJ and AMC (POEM Group, 1992; Zodiatis et al., 2005; Lascaratos et al., 1999). The southern part of the basin is characterised by some recurrent or permanent sub-basin eddies. The anticyclonic Ierapetra Eddy (IE), induced by summer northerly Etesian winds (Millot and Taupier-Letage, 2005; Hamad et al., 2005, 2006; Gaines et al., 2006; Amitai et al., 2010), is located south-east of Crete with a diameter of 100–150 km (Hecht and Gertman, 2001). The anticyclonic Mersa-Matruh Eddy (MME), according to Brenner (1989), is generated in summer close to the Egyptian coast by an unstable meander of the LEC. According to other studies, this feature is a permanent eddy (Robinson et al., 1991; Tziperman and Malanotte-Rizzoli, 1991; Malanotte-Rizzoli and Bergamasco, 1991) or a meander of the MMJ (Larnicol et al., 2002). The eastern LSB is dominated by two recurrent anticyclonic eddies: the Cyprus Eddy (CE) and Shikmona Eddy (ShE). The CE is a recurrent dynamic feature characterised by seasonal variability in shape, dimension and position (Zodiatis et al., 2005). The ShE represents a complex system, composed of several cyclonic and anticyclonic eddies, in which the positions, sizes and intensities vary markedly (Ayoub et al., 1998; Zodiatis et al., 1998; Gertman et al., 2007). The ShE is considered as either permanent (Hecht et al., 1988; Ozsoy et al., 1989) or recurrent (Robinson et al., 1991; Zodiatis et al., 2005), and is encountered in all seasons except in winter (Tziperman and Malanotte-Rizzoli, 1991), or generated in summer (Roussenov et al., 1995). The Latakia Eddy (LTE), located between Cyprus and the Syrian coast, is indicated by Hamad et al. (2005) as a cyclonic feature partly generated by the ShE and by the coastline orientation, and from Gerin et al. (2009) as mainly created by topography; according to Zodiatis et al. (2003) the LTE is generated by the interaction of the northward current along the Lebanon and Syria coasts with the MMJ.

The main characteristic, widely acknowledged by all the oceanographers, is the complexity and multi-scale system of the LSB circulation. The surface circulation consists of complicated flow patterns, characterised by regions with strong eddy kinetic energy (Robinson et al., 1987; Pujol and Larnicol, 2005; Pascual et al., 2007; Amitai et al. 2010), strong offshore and along-slope currents (Robinson et al., 1991; Hamad et al., 2005; Millot and Taupier-Letage, 2005, Zodiatis et al., 2010) and several multi-scaled eddies (Özsoy et al., 1991; Pinardi and Masetti, 2000; Fusco et al., 2003; Zodiatis et al., 2005).

The main controversial aspect of the LSB surface circulation is about the pathway of the surface waters coming from the west. According to the POEM group (Physical Oceanography of the Eastern Mediterranean) circulation map (Robinson et al., 1991; POEM Group, 1992), the surface and sub-surface waters of Atlantic origin flow in the LSB as an open sea central eastward current (Zodiatis et al., 2010). This continues as MMJ and splits in several branches: some branches turn anticyclonically to feed clockwise circulation features such as the MME and the ShE (Malanotte-Rizzoli and Robinson, 1988; Robinson et al., 1991, 2001; Robinson and Golnaraghi, 1993; Malanotte-Rizzoli et al., 1997). Other branches turn cyclonically southwest of Cyprus, forming the RG, the West Cyprus Eddy and the AMC. The path of MMJ is supported by high resolution in-situ CTD (Zodiatis et al., 2005, 2010) and glider observations (Hayes et al., 2010).

An alternative surface circulation map, based on the analysis of long time series of satellite SST images (Hamad et al., 2005, 2006; Millot and Taupier-Letage, 2005), shows that the surface waters flow as a slope current all around the basin. The southern part of this slope current (LEC) is markedly unstable and generates numerous instability features (anticyclonic eddies) similarly to the situation in the Western Mediterranean basin (Algerian Current; Millot, 1999). According to these analyses, the MMJ described by the POEM group corresponds to the northern limbs of the anticyclonic eddies generated by the along-slope current. The path of surface waters along the Libyo-Egyptian slope is supported by satellite-tracked drifter data (Gerin et al., 2009; Millot and Gerin, 2010), in-situ XBT data (Manzella et al. 2001; Fusco et al., 2003) and numerical simulations (Alhammoud et al., 2005).

The primary purpose of this paper is to provide a thorough description of the surface circulation in the LSB, using the historical and NEMED (North East Mediterranean) project drifter data, so as to clarify some ambiguities about the pathways of surface waters in this area. The NEMED project was carried out by OGS (Istituto Nazionale di Oceanografia e Geofisica Sperimentale) in collaboration with OC-UCY (Oceanography Centre—University of Cyprus) and IOLR (Israel Oceanographic and Limnological Research). The goal of NEMED was to measure the surface currents in the LSB during 2009–2011, with particular focus to the eastern and northern areas of the sub-basin (Fig. 1). NEMED data were added to the historical drifter data of the LSB to provide a 18-year (November 1992–March 2011) exhaustive description of the circulation and dynamical structure in this area. The drifter data yield an accurate but irregular spatial and temporal sampling of near-surface currents, therefore they were used in conjunction with regularly sampled satellite-derived sea level anomalies and ocean surface wind velocities to assemble time-averaged maps of the near-surface geostrophic velocity. The LSB drifter/satellite velocity dataset, computed employing the results obtained by Menna et al. (2010) and Poulain et al. (2012), was used to produce the pseudo-Eulerian maps of mean surface geostrophic flow, eddy variability and energy levels.

The second purpose of this paper is to improve the knowledge on the sub-basin circulation and eddy generation in the eastern LSB. The study is mainly focused on the currents trapped on the topographic slope and on the seasonal and interannual variability of specific sub-basin and mesoscale eddies in the period 2009–2010.

The paper is organised as follows: drifter characteristics, information on drifter and remotely sensed altimetry data and details on the data processing are included in Section 2, followed by a description of the methods used to compute the surface geostrophic flow field and to define the sub-basin scale features in the LSB. Pseudo-Eulerian statistics, seasonal characteristics and eddy variability are presented in Section 3. The conclusions are summarised in Section 4.

2. Data and methods

2.1. Data

2.1.1. Drifter data and processing

The drifters used in the NEMED project are the Global Drifter Programme (GDP) drifters drogued with a holey sock centred at 15-m depth. The GDP drifter is similar to the Surface Velocity Programme (SVP) drifter design (Lumpkin and Pazos, 2007). It is equipped with a sea surface temperature sensor and a tension sensor that allows checking the presence of the drogue. A total of 34 drifters were deployed from research vessels and ships of opportunity (Ferries, Tara expedition) between July 2009 and October 2010, along the Limassol-Port Said transect, south of Cyprus and west of Israel (see Fig. 1). Deployments were organised on a seasonal basis. More details about the NEMED drifters are available at the web page http://nettuno.ogs.trieste.it/sire/drifter/database/NEMED/index.html.

The historical drifter dataset, spanning from November 1992 to April 2008, composed of 139 drifters, includes data of the EGITTO project (2005–2008; see Gerin et al., 2009) and data of different databases (Mediterranean Surface Drifter Database; METEOFRANCE; NAVO). These data come from a variety of drifter designs, including the Coastal Ocean Dynamics Experiment (CODE) drifter, the Compact Meteorological and Oceanographic Drifter (CMOD) and the SVP drifter. The SVP units are sorted into 3 different categories according to the drogue presence: drogued, undrogued and unknown (no information on drogue presence).

The NEMED and historical drifter observations were grouped together to create the complete LSB drifter dataset. Among all the drifters deployed in the Mediterranean Sea, we have considered both drogued and undrogued drifters to study quantitatively the circulation in the surface layer (0–15 m). Technical details about these buoy systems can be found in Poulain et al. (2004) and at the web page: http://poseidon.ogs.trieste.it/drifter/database_med/html/scidoc.html.

All drifters were tracked by the Argos Data Collection and Location System (DCLS) carried by the NOAA polar-orbiting satellites. Drifter locations have accuracy better than 1500 m (Carval et al., 2008). The drifter position time series were first edited from spike and outliers, then linearly interpolated at regular 2-h intervals using the kriging technique (optimal interpolation; Hansen and Poulain, 1996; Poulain et al., 2004). The interpolated positions were low-pass filtered using a Hamming filter (cut-off period at 36 h) in order to remove higher frequency current components (tidal and inertial currents) and were finally sub-sampled at 6-h intervals. Velocity components were then estimated from centred finite differences of 6-h sub-sampled positions.

The low-pass filtered and interpolated tracks of the LSB dataset are depicted in Fig. 2; light and dark grey tracks depicts NEMED and historical drifter trajectories, respectively. The geographical coverage is rather dense in the southern LSB, whereas the areas west and north of Cyprus, and east of Rhodes have only scarce drifter observations. The entire dataset includes 47372 6-h data points, corresponding to more than 31.7 drifter-years. The temporal distribution of the data, between 8 November 1992 and 21 March 2011, is depicted in Fig. 3. The maximum number of drifters operating simultaneously occurred in April 2006 with 19 units; the data distribution shows three major temporal gaps without observations (between March 1998 and January 2002, between April 2004 and November 2005, between April 2008 and July 2009).

2.1.2. Sea surface height anomaly data

The altimetry data used for this study are gridded (1/8° Mercator projection grid) Ssalto/Duacs weekly, multi-mission,

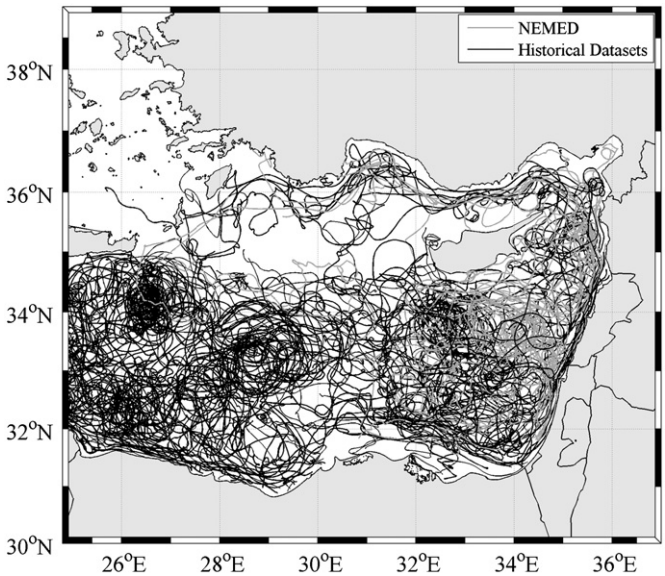

Fig. 2. Low-pass filtered drifter trajectories between November 1992 and March 2011. Light grey tracks correspond to NEMED dataset; dark grey tracks show the historical drifter datasets.

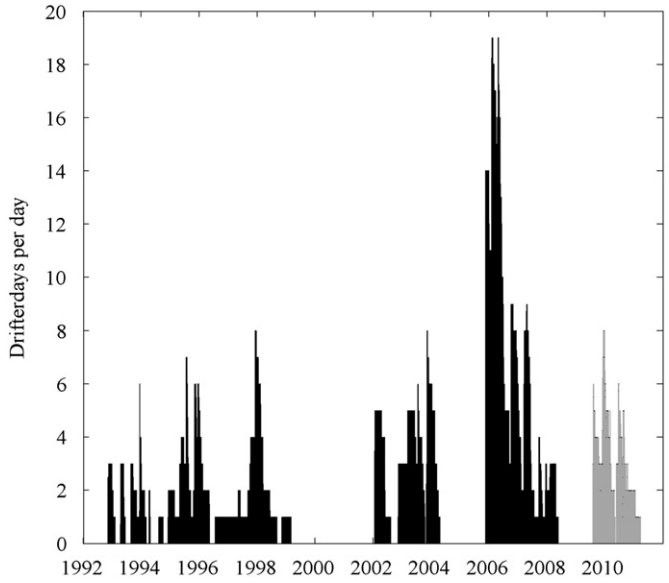

Fig. 3. Temporal distribution of the NEMED (light grey) and historical drifter datasets (dark grey), spanning 8 November 1992 to 21 March 2011.

delayed time (quality controlled) products from AVISO (SSALTO/DUACS users handbook 2010). Among the available versions of the delayed time products we have selected the reference data series, based on two satellite missions (Jason-2/Envisat or Jason-1/Envisat or Topex/Poseidon/ERS) with the same groundtrack. Thus the reference series are homogeneous during the available time period. Absolute dynamic topography (ADT), sea level anomaly (SLA) and corresponding anomalies of surface geostrophic velocities data were downloaded. SLA data are defined with respect to a 7-year mean (1993–1999). The ADT is the sum of SLA and Synthetic Mean Dynamic Topography (SMDT), estimated by Rio et al. (2007) over the 1993–1999 period. The time span for the delayed time AVISO data is from 14 October 1992 to 31 March 2011.

2.2. 2 Methods

2.2.1. Wind-driven and geostrophical currents

Wind-driven or Ekman currents ($\boldsymbol{U_{wind\text{-}driven}}$) were readily computed using the following linear regression model (Poulain et al., 2012):

$$\boldsymbol{U}-\boldsymbol{U_{AGV}}=\boldsymbol{U}_{\text{wind-driven}}+\boldsymbol{error}=\boldsymbol{\beta exp}(i\theta)\boldsymbol{W}+\boldsymbol{error}; \quad (1)$$

where $\boldsymbol{U}$ is the drifter velocity; $\boldsymbol{U_{AGV}}$ is the absolute geostrophic velocity (AGV) derived from ADT products, linearly interpolated to locations and times of drifter observations; $\boldsymbol{\beta}$ is a real constant and $\boldsymbol{\theta}$ is the angle (positive anticlockwise) which represent, respectively, the estimations of intensity and the direction of drifter wind-driven currents with respect to the wind speed; $\boldsymbol{W}$ is the Cross-Calibrated, Multi-Platform (CCMP) ocean surface wind velocity interpolated at the drifter locations and times (Atlas et al., 2009). $\boldsymbol{U}$, $\boldsymbol{U_{AGV}}$ and $\boldsymbol{W}$ are vectors and are expressed as complex numbers. The model was applied to the different drifter designs separately, over the whole Mediterranean Sea, and the results are summarised in Table 2.

In our study we adopted the relationship between wind-driven currents and wind speed shown in Table 2 to compute wind-driven currents. More details about the wind data and the regression model can be found in Poulain et al. (2012). The regression of Eq. (1) was also applied without removing the absolute surface geostrophic currents $\boldsymbol{U_{AGV}}$. The results are essentially identical to those listed in Table 2, except that the explained velocity variance is smaller, varying between 1 and 19% (Menna et al., 2010).

Table 2
Results of the regression model (Eq. 1) applied to extract the wind-driven currents from the velocities of the different types of drifters (Poulain et al., 2012). R^2 is the coefficient of determination and N is the number of observations in the LSB.

Drifter type	$\beta e^{i\theta}$	R^2 (%)	N
CODE	$0.01\exp(-33^\circ i)$	11	4542
SVP drogued	$0.005\exp(-34^\circ i)$	1	9735
SVP undrogued	$0.01\exp(-26^\circ i)$	22	7987
SVP unknown	$0.007\exp(-34^\circ i)$	5	17875
CMOD	$0.02\exp(-18^\circ i)$	27	7233

The wind-driven currents were then subtracted from drifter velocity measurements to obtain the geostrophic components ($\boldsymbol{U_{DG}}$):

$$\boldsymbol{U_{DG}}=\boldsymbol{U}-\boldsymbol{U}_{\text{wind-driven}} \quad (2)$$

The CCMP wind products are available from July 1987 to December 2010. Therefore, $\boldsymbol{U_{wind\text{-}driven}}$ and $\boldsymbol{U_{DG}}$ cannot be evaluated using the drifter data after 2010. Hence all the results presented hereafter corresponded to the period November 1992–December 2010. Note that the wind-driven currents estimated here include the contribution of slippage of the drifter induced directly by wind. Slippage is more important for the CMOD and SVP undrogued drifter. This explains the different values of $\boldsymbol{\beta}$ and $\boldsymbol{\theta}$ in Table 2 (see also Poulain et al., 2009).

2.2.2. Unbiased geostrophic velocities and pseudo Eulerian statistics

The pseudo-Eulerian statistics of the drifter geostrophic ($\boldsymbol{U_{DG}}$) and wind-driven ($\boldsymbol{U_{wind\text{-}driven}}$) velocities are defined as 'biased', according to the nomenclature used in Centurioni et al. (2008, 2009) and Poulain et al. (2012). In this context the word 'biased' corresponds to statistics which depend on the specific non-uniformly sampled (in space and time) drifter data. On the other hand, remotely sensed SLA data can be used to estimate statistics of the surface geostrophic circulation with less biases since they are more regularly sampled in space and time (Centurioni et al., 2008; Poulain et al., 2012). The main drawbacks are that altimetry data are generally low-pass filtered (due to the satellite subtrack patterns and repeat times) and inaccurate in coastal areas and in the resolution of mesoscale features. In addition, AVISO products are interpolated on a regular grid with mesh size of 1/8° every week. Interpolation and sampling errors are not negligible but the combination of drifter and altimetry data provides a more accurate representation of the mean circulation than computation performed from each dataset alone (Centurioni et al., 2008; Poulain et al., 2012). Following the above considerations, the drifter and satellite altimetry geostrophic velocities were combined to construct a regularly sampled dataset of observations. The pseudo-Eulerian statistics computed on the combined geostrophic velocity field are defined as 'unbiased'. Drifter and satellite altimeter data were averaged in the same geographical bins and time intervals.

In Poulain et al. (2012) the velocities obtained from altimetry and from the drifters over the whole Mediterranean Sea were averaged in overlapping (50%) geographical bins of $1^\circ \times 1^\circ$ organised on a 0.5° grid and in time intervals of one week. This bin-size was chosen as a compromise to resolve the basin and sub-basin circulation of the Mediterranean Sea but the relative maps of the mean unbiased circulation are unable to discriminate the formation mechanism and evolution of the anti-cyclonic features in the LSB and their possible interaction and generation by the coastal current. In this work, in order to focus on the aspects of LSB circulation not studied in Poulain et al. (2012), a higher bin-resolution was chosen. The weekly sampling period of the anomalies of surface geostrophic velocities,

obtained from AVISO, was preserved whereas the spatial grid of 1/8° were reduced to 0.25° × 0.25° by sub-sampling to create $\boldsymbol{U_{SLA}}$. To homogenise satellite altimetry and in-situ drifter data, the drifter velocities were also averaged in non-overlapping bins of 0.25° × 0.25° and over 7-day ($\boldsymbol{U_{DG}}$). The spatial bins and time intervals with less than 3 drifter observations were not considered. The spatial distribution of the number of weeks with more than 3 drifter observations over the period 1992–2010 is shown in Fig. 4. The bins with a high number of observations (> 25) are located in the western and eastern LSB.

Within each spatial bin the following regression model was applied (Poulain et al., 2012):

$$\boldsymbol{U_{DG}} = \boldsymbol{A}\boldsymbol{U_{SLA}} + \boldsymbol{B} + \boldsymbol{error}, \quad (3)$$

where $\boldsymbol{U_{SLA}}$ is the bin averaged (0.25° × 0.25° × 1 week) anomalies of surface geostrophic velocities, concurrent with $\boldsymbol{U_{DG}}$. The unknown coefficients $\boldsymbol{A}$ and $\boldsymbol{B}$ can be estimated minimising the error. The slope $\boldsymbol{A}$ is the local adjustment of amplitude of AVISO velocity $\boldsymbol{U_{SLA}}$ (Niiler et al., 2003). Over the time period considered for the definition of SLA (1993–1999), the mean of $\boldsymbol{U_{SLA}}$ is zero and $\boldsymbol{B}$ coincide with the time-mean drifter circulation. For any other period, the mean of $\boldsymbol{U_{SLA}}$ is not zero and $\boldsymbol{B}$ is the offset between $\boldsymbol{U_{SLA}}$ and $\boldsymbol{U_{DG}}$. Following Poulain et al. (2012), the slope $\boldsymbol{A}$ was subsequently low-pass filtered in 0.75° × 0.75° overlapping bins to remove insignificant noise. Eq. (3) estimates the optimal values of the coefficients $\boldsymbol{A}$ and $\boldsymbol{B}$ in the period 1992–2010, in which satellite, wind and drifter data are available. The magnitude of $\boldsymbol{A}$ (not shown) varies between 0 and 3.5; it exceeds 1.5 in the region south of Crete, along the slope and in the regions west and south-west of Cyprus. The magnitude of offset $\boldsymbol{B}$ (not shown) is about 15 cm/s in the slope current and south of Cyprus; it exceeds 20–25 cm/s in the Ierapetra and Mersa-Matruh eddies (Poulain et al., 2012).

The amplitude of the vector complex correlation (Kundu, 1976) between $\boldsymbol{U_{DG}}$ and $\boldsymbol{U_{SLA}}$ (not shown) reached large values (above 0.5) in most of the LSB. The 'unbiased' mean geostrophic velocities can be estimated using the following model:

$$\langle \boldsymbol{U_G} \rangle_{\boldsymbol{u}} = \boldsymbol{A}\langle U_{SLA} \rangle_u + \boldsymbol{B}, \quad (4)$$

where $\langle\,\rangle_{\boldsymbol{u}}$ indicates "unbiased" temporal averages in each spatial bin and $\boldsymbol{U_G}$ is the surface geostrophic current. The relationship between drifter velocities and satellite sea level anomaly, estimated from 18 years of concurrent data in Eq. (3), can be used to estimate the unbiased geostrophic currents $\langle \boldsymbol{U_G} \rangle_{\boldsymbol{u}}$ in the whole period in which $\boldsymbol{U_{SLA}}$ is available.

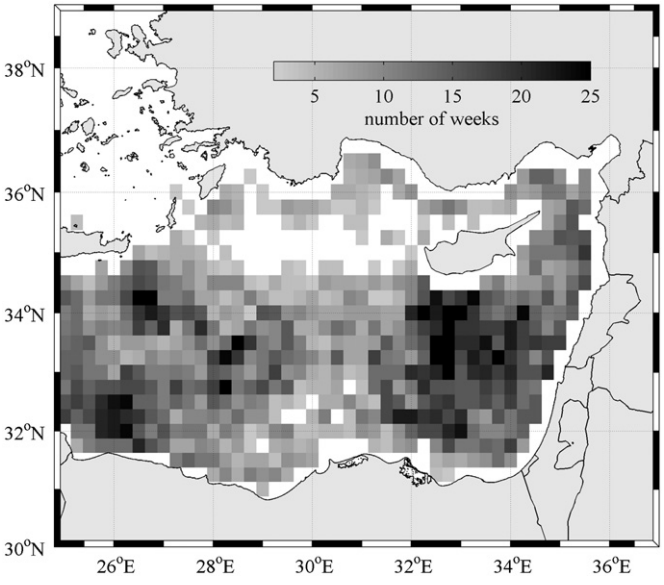

Fig. 4. Number of weeks in which 6-hourly drifter observations occur, divided in 0.25° × 0.25° spatial bins. Bins with less than 3 weeks of data are not considered.

Pseudo-Eulerian statistics were computed on regularly sampled (0.25° × 0.25° × 1 week) geostrophical velocities. Maps of mean circulation, kinetic energy of the mean flow per unit mass (mean kinetic energy—MKE) and of mean kinetic energy of the residuals per unit of mass (eddy kinetic energy—EKE) were constructed (Poulain, 2001).

The residuals of geostrophic velocity field were evaluated removing the mean unbiased velocity $\langle \boldsymbol{U_G} \rangle_{\boldsymbol{u}}$ from each weekly value of $\boldsymbol{U_G}$:

$$\boldsymbol{U'_G} = \boldsymbol{U_G} - \langle \boldsymbol{U_G} \rangle_u; \quad (5)$$

then, the EKE was defined as

$$\mathrm{EKE} = 1/2\langle U'^2_G + V'^2_G \rangle_u. \quad (6)$$

In order to assess the seasonal variations of geostrophic currents, the pseudo-Eulerian statistics were also computed for two extended seasons of 6 months duration.

2.2.3. Sub-basin eddies in the eastern LSB

The interannual variability of sub-basin eddies in the eastern LSB was investigated in terms of kinetic energy of velocity residuals, evaluated for each weekly value of $\boldsymbol{U'_G}$ and defined as

$$\mathrm{KE} = 1/2U'^2_G + V'^2_G. \quad (7)$$

The Hovmoller diagrams of the KE in the period 1993–2010 were computed for the CE, ShE and LTE regions. The generation and evolution of above mentioned eddies were described using the geostrophic velocities $\boldsymbol{U_G}$ and the NEMED drifter tracks in the period summer 2009–fall 2010.

3. Results and discussion

3.1. Pseudo-Eulerian statistics of the unbiased geostrophic currents

The unbiased pseudo-Eulerian mean velocity field (Fig. 5a), obtained using Eq. (4), depicts the well known anticlockwise circulation around the whole basin, in agreement with the historical scheme suggested by Nielsen (1912) and Ovchinnikov (1966). The along-slope current flows off the Egypt, Israel and Lebanon coasts with mean speed of 15–20 cm/s; its velocity increases in the Cyprus–Syria Passage and in the northern Levantine sector (Cilician and Antalya basins), with mean values exceeding 25 cm/s. The southern and eastern limbs of the along-slope current generate the Egyptian eddies (EE) and the ShE as described by Hamad et al. (2005, 2006) and Gertman et al. (2007) respectively, whereas the interaction between this current and the MMJ generates the LTE in agreement with Zodiatis et al. (2003). The northern limb of the coastal current (Cilician Current—CC—and AMC) flows westward along the Turkish coast and delineates the northern boundary of the RG. The EE eddies are characterised by typical speeds between 10 and 15 cm/s; the ShE main anticyclonic lobe reaches a bin-averaged speed of 20 cm/s, whereas the velocities of a secondary cyclonic lobe, south of the main eddy, are weaker (less then 10 cm/s); the LTE has a typical speed of about 10 cm/s.

A meandering eastward current, which can be identified as the MMJ is located between 34°–35°N and 28°–35°E (Fig. 5a); a branch of this current turns into cyclonic and anticyclonic eddies, as documented by several authors in the past years (Malanotte-Rizzoli and Robinson, 1988; Robinson et al., 1991, 2001; Robinson and Golnaraghi, 1993; Malanotte-Rizzoli et al., 1997); another branch interacts with the northward along-slope current. The MMJ brushes the southern limb of the RG and the northern limbs of the MME, CE

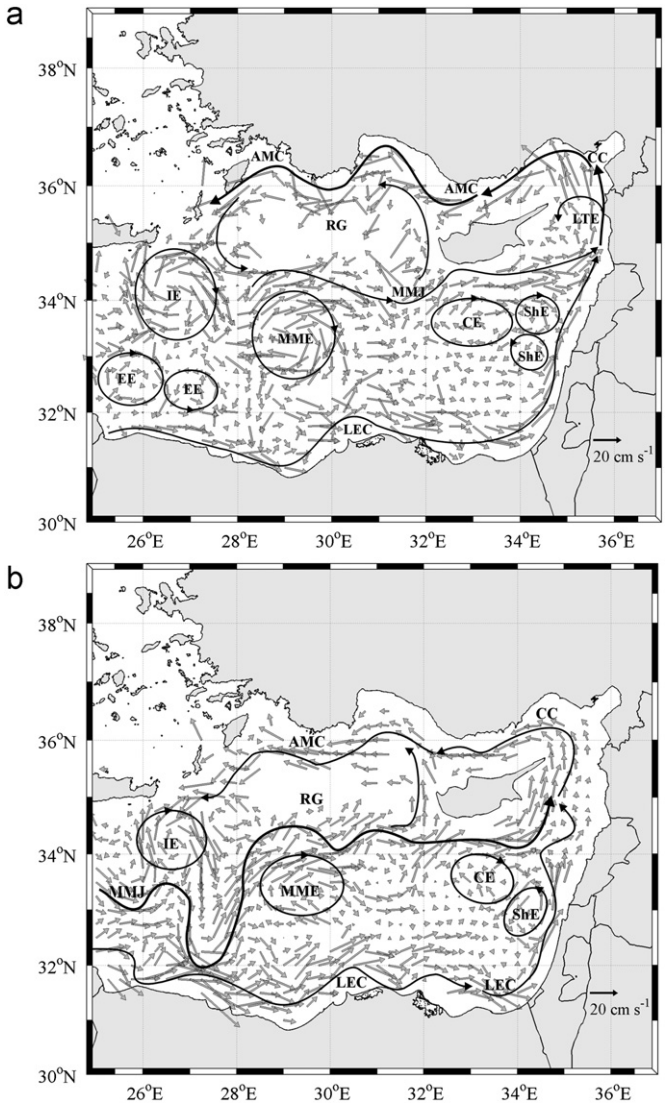

Fig. 5. Pseudo-Eulerian mean velocity field (a) in the period 1992–2010 (dark grey), obtained from the unbiased geostrophic currents in bins of 0.25° × 0.25°. Mean of absolute geostrophic velocities (Rio et al., 2007) (b) in the same period and bins of (a); Black lines emphasise the main currents and sub-basin eddies in both panels.

and ShE with speeds of 15–20 cm/s and joins into the coastal current in the Latakia region. The CE, located southwest of Cyprus in the vicinity of the Eratosthenes Seamount, is an anticyclonic flow characterised by an intense northern limb (speed of 15–20 cm/s) and a weak (speeds of 5 cm/s) southern limb. The MME is an anticyclonic feature with a diameter of ~150–200 km and mean speeds larger than 20 cm/s. More to the west, in the region southeast of Crete, the circulation is dominated by the persistent anticyclonic IE, with speeds between 15 and 30 cm/s.

The mean geostrophic current field estimated with our unbiased method (Eq. (4)) and described above (Fig. 5a), was compared with the mean surface absolute geostrophic velocities ($\boldsymbol{U_{AGV}}$), directly derived from ADT. Fig. 5b shows the $\boldsymbol{U_{AGV}}$ in the same period (1992–2010) and in the same bins selected for the unbiased geostrophic currents. The $\boldsymbol{U_{AGV}}$ currents in the Mediterranean Sea are estimated using the dynamic topography outputs from MFSTEP (Mediterranean Forecasting System: Toward Environmental Predictions) model (Demirov et al., 2003), locally improved with the mean geostrophic circulation obtained by combining drifter velocities and altimetric data (Rio et al., 2007; Rio and Hernandez, 2004). The comparison between $\boldsymbol{U_{AGV}}$ (Fig. 5b) and the unbiased map (Fig. 5a) reveals substantial differences. The $\boldsymbol{U_{AGV}}$ currents are more intense (maximum speed larger than 35 cm/s) along the Egyptian slope and less intense (10–20 cm/s) along the Syrian and Turkish slope (in the AMC), with respect to the unbiased map; the diameters of IE and MME appear to be reduced by about 25 km in the $\boldsymbol{U_{AGV}}$ map. The $\boldsymbol{U_{AGV}}$ currents show distinctly the MMJ pathway throughout the basin (Rio et al., 2007; Amitai et al., 2010), characterised by a southward fast meander (speeds of 20–25 cm/s) between IE and MME (27°–28°E) reaching the LEC, in contrast to the unbiased map where this fast jet is not recognisable. The results of the unbiased method in the LSB can be considered more realistic and accurate than the $\boldsymbol{U_{AGV}}$ because they are mainly based on in-situ drifter data. On the other hand, the $\boldsymbol{U_{AGV}}$ currents are mainly based on MFSTEP outputs and a reduced set of in-situ drifter data, used to improve the model results, mainly located in regions of the Mediterranean Sea (Adriatic and Ionian Seas; see Rio et al., 2007) that not include the LSB.

Fig. 6 shows the maps of MKE and EKE related to the unbiased geostrophic currents depicted in Fig. 5a. The LSB is characterised by areas with strong MKE (Fig. 6a), located in the northern border of the IE (maximum values larger than 300 cm^2/s^2), in the MME (between 250 cm^2/s^2 and 350 cm^2/s^2) and in the AMC (maximum

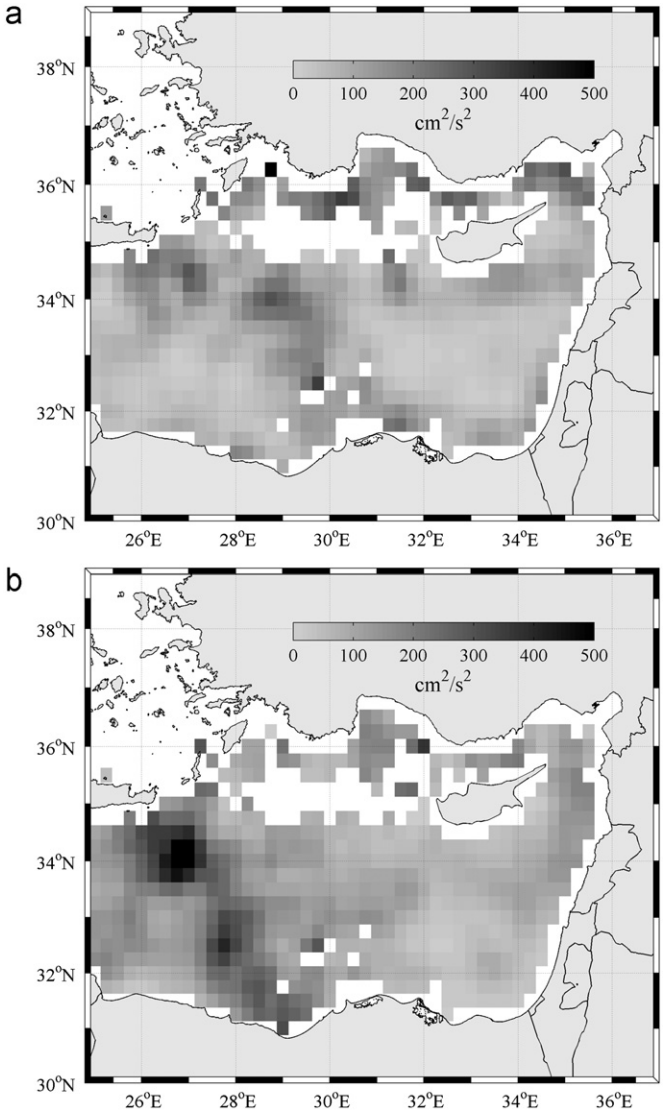

Fig. 6. Unbiased statistics of mean kinetic energy (a) and eddy kinetic energy (b) of the surface geostrophic currents.

values larger than 400 cm^2/s^2), in accordance with the energy levels estimated by Mauerhan (2000), Poulain et al. (2012) and Gerin et al. (2009). The EKE field (Fig. 6b) gives information about the unbiased variance of velocity residuals; it suggests that the IE region is characterised by highly variable currents (values larger than 600 cm^2/s^2 in the core of IE), as well as the Antalya basin. The region between IE and MME (31.5°–33.5°N–28°–30°E) is also characterised by high current variability, with EKE between 250 cm^2/s^2 and 400 cm^2/s^2, as the result of the interaction between the MMJ meandering and the instability of current off the Israel, Lebanon and Syrian coasts. In the eastern part of LSB, the areas with remarkable EKE values (250–300 cm^2/s^2) are located on the border among the CE and the ShE lobes and in the Latakia region. The geographical distribution of EKE is comparable to the results of Pujol and Larnicol (2005) and Pascual et al. (2007).

The unbiased statistics in the LSB harmonise the two different circulation maps described in previous studies (see Section 1). According to Fig. 5a the presence of along-slope current does not exclude the existence of a cross basin current (MMJ) and vice-versa; both currents play a crucial role in the basin and sub-basin scale circulation of the LSB.

3.2. Seasonal characteristics of the unbiased geostrophic current statistics

The seasonal variability of the geostrophic velocities field was estimated dividing the dataset in two extended seasons, based on the examination of monthly-averaged geostrophic velocities and ADT maps (not shown). These maps reveal that the speeds and sea level heights in winter are comparable to the spring values, whereas the summer values are comparable to those in fall. On this basis, the extended winter was defined as the period January–June and the extended summer as the period July–December.

The salient seasonal variations in the pseudo-Eulerian statistics are depicted in Fig. 7. The IE appears weaker in winter (Fig. 7a), confirming the result of Gerin et al. (2009), with speeds less than 5 cm/s in the southern limb (MKE between 50 cm^2/s^2 and 100 cm^2/s^2) and maximum values of 20–25 cm/s in the eastern limb (MKE larger than 200 cm^2/s^2); it is stronger in summer (Fig. 7b) with speeds as large as 30–40 cm/s and values of MKE larger than 300 cm^2/s^2. The MMJ is weaker in winter (maximum speeds of 20 cm/s; maximum MKE values of 250 cm^2/s^2) and most vigorous in summer (maximum speeds larger than 30 cm/s and MKE of 250–350 cm^2/s^2); summer speeds are in agreement with the results of Zodiatis et al. (2005). The eastern LSB and the along-slope current show similar characteristics in both the extended seasons. The EKE levels (Fig. 7c and d) are generally higher in summer in particular in the IE, in the area between IE and MME and in the Latakia region. The seasonal variability of EKE levels in the LSB is comparable to the estimates of Amitai et al. (2010).

3.3. Interannual variability of eastern Levantine

In this sub-section we focus on the eastern part of the LSB to describe the main characteristics and variability of the dynamical

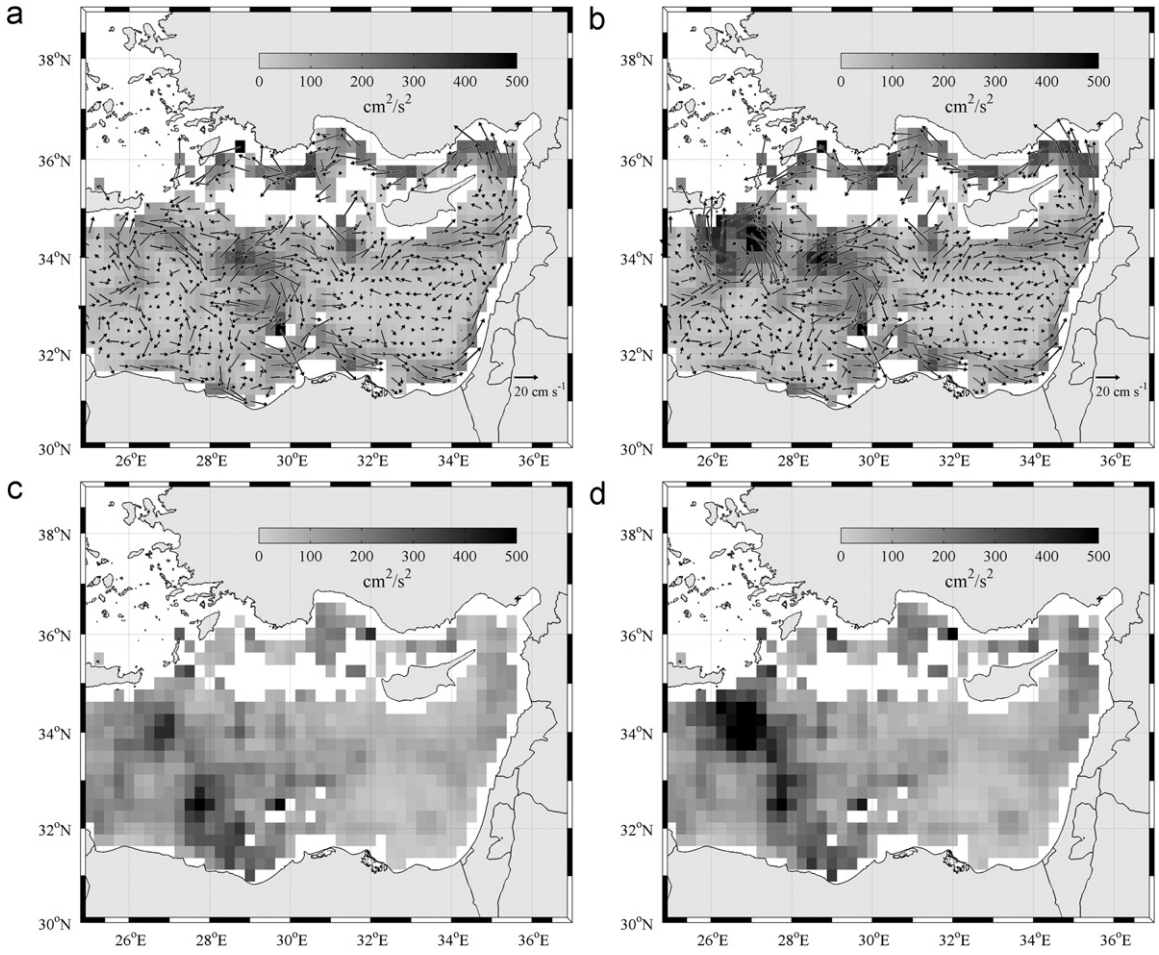

Fig. 7. Pseudo-Eulerian statistics for the extended seasons. Mean flow and mean kinetic energy in the extended winter (a) and in the extended summer (b); seasonal unbiased statistics of eddy kinetic energy in the extended winter (c) and in the extended summer (d).

structures that govern the circulation. The Hovmoller diagram of KE (Figs. 8 and 9) is a useful way to depict the spatio-temporal variability in different regions of the eastern LSB. The range of the colorbars depicted in Figs. 8 and 9 (0–400 cm^2/s^2) represents the best compromise to plot together dynamical structures characterised by a wide range of values of KE (between 150 and 700 cm^2/s^2).

The diagram in Fig. 8a, computed by meridionally averaging each KE value between 33°N and 35°N, includes the sub-regions of the CE and ShE. The lower boundary (32°–33.5°E) of each yearly subplot captures the activity of the CE, characterised by events of high KE (fall 1997; 1998–2003; winter 2004; spring 2005–2007; fall 2006; spring–summer–fall 2010) with values larger than 200 cm^2/s^2, alternated with periods of low energy (e.g. 1993–1996; spring–summer–fall 2004; 2008–2009). Seasonal and inter-annual changes in intensity and location of the CE are well documented in Fig. 8a, confirming the results of Groom et al. (2005) and Zodiatis et al. (2005). Between 33.5°–35.5°E, the diagram depicts the ShE generation area (as defined by Gertman et al., 2007) and the upper part of each yearly subplot follows the coast line (35°E–35.5°E). The along-slope meandering that generates ShE (Gertman et al., 2010) has a periodic nature with KE signal larger than 700 cm^2/s^2 during late summer, fall and winter and from 200 cm^2/s^2 to 500 cm^2/s^2 during spring and early summer. When the eddy moves westward it dissipates a part of its energy and assumes typical KE values of 200–300 cm^2/s^2. The most intense activity of ShE is observed between 1998 and 2005. Occasionally the circulation of the southeast LSB is dominated by a single anticyclonic structure (1995, 1996, January–June 1999, July–November 2001, August–December 2004, 2007), with a diameter of 250–300 km, that covers the CE and the ShE regions. Examples of the two different pathways, that occur in the CE and ShE area, are provided in Fig. 8b (two noticeable anticyclonic features) and Fig. 8c (one large anticyclonic eddy).

The diagram in Fig. 9a, computed by meridionally averaging KE values between 34.5°N and 36°N, includes the sub-region of the LTE. The KE in this area is influenced by the interaction of the MMJ with the northward coastal current. The KE signal shows generally higher values in summer and fall (larger than 500 cm^2/s^2), when the MMJ is more intense, and lower values (less than 200 cm^2/s^2) in spring and winter. A winter intensification of LTE is observed in the periods 2001–2006 and 2008–2010. The circulation in the Latakia region is mainly dominated by a cyclonic pathway, sometimes broken by periods (weeks or months) of inverse circulation. The inversions in surface circulation, from cyclonic to anticyclonic regimes, are triggered by the interaction of MMJ with the northward meandering along-slope current. Usually the meanders of the coastal current are located in the ShE generation area, between 32°N and 35°N; sometimes they move northward and end up trapped between the Syrian and the eastern Cyprus coasts, inducing the inversions of the flow pattern. These anticyclonic events, generally related to significant increase of the KE, occurred in the following periods (Fig. 9a): December 1993; December 1994; July–August 1997; October 1997; July–August 1998; October–November 1999; July 2000; November 2000; March–April 2001; July–December 2001; January–February 2002; December 2002; June–October 2003; January 2004; March 2004; September–December 2004; January–February 2005; July–December 2005; February–April 2006; January 2008; May–April 2008; July–August 2008; March 2010; August–October 2010.

Examples of anticyclonic and cyclonic regimes in the Latakia basin are shown in Figs. 9b and c, respectively.

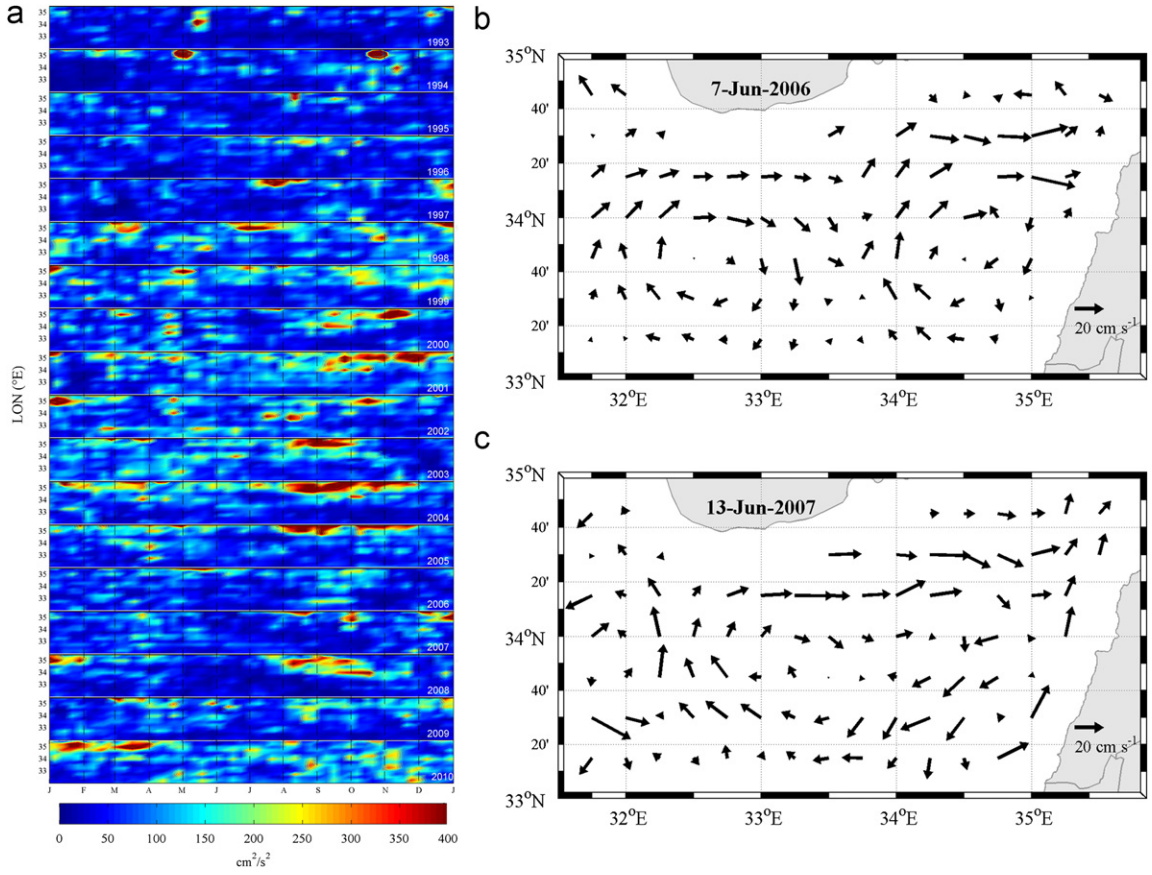

Fig. 8. Hovmoller diagrams of KE over Cyprus and Shikmona eddies (a). The diagrams are constructed by averaging KE meridionally between 33°N and 35°N. Snapshot with two different eddied (b): the CE on left and the ShE on right. Snapshot of geostrophic currents with a single anticyclonic eddy (c).

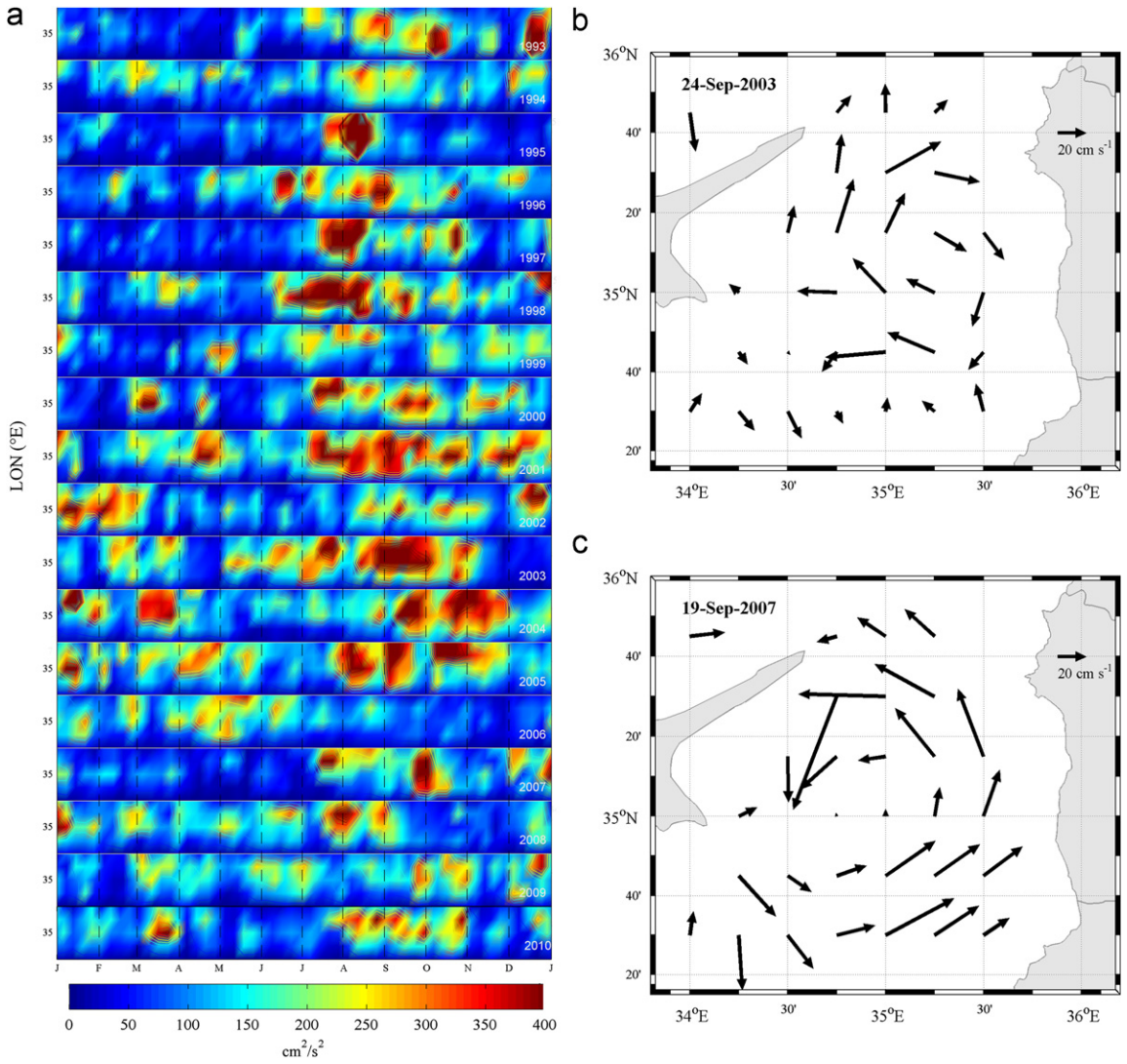

Fig. 9. Hovmoller diagrams of KE over Latakia area (a). The diagrams are constructed by averaging KE meridionally between 35°N and 36.5°N. Snapshot of geostrophic currents with anticyclonic (b) and cyclonic (c) pathways.

3.4. *Temporal evolution of sub-basin eddies in the eastern Levantine*

In this sub-section we use NEMED drifter tracks, superimposed with the unbiased geostrophic currents, to describe the temporal evolution of the ShE, CE and LTE in the period spanning from summer 2009 to fall 2010. The panels in Figs. 10–13 contain four-weekly unbiased mean geostrophic currents maps, superimposed with concurrent drifter trajectories (coloured lines). Speed values indicated in the following text are referred to geostrophic velocities derived from Eq. (3).

In summer–fall 2009 (Fig. 10), drifter tracks depict the generation of the ShE (Fig. 10a) as a pinched off meander from the instability of the northward current along the Israeli–Lebanese coast (speeds of 15–20 cm/s); in the same weeks a drifter deployed south of Cyprus is captured by the ShE circulation and moves in the neighbourhood of the eddy core. More to the west (33.5°–34.5°N; 32°–33°E) the circulation is governed by the CE, whose diameter is ~100 km and the mean speed along the border is ~20 cm/s. In the Latakia area (Fig. 10b) drifter tracks describe a large cyclonic circulation trapped between the Syrian coast (speeds larger than 30 cm/s) and the eastern Cyprus coast (speeds of 5–10 cm/s). The ShE (33.2°–34°N; 33.8°–35°E) rotates steadily (speeds between 20 and 33 cm/s) and drifters carry out 7 full cycles around the eddy core (diameter of ~100 km). In early fall (Fig. 10c), drifters leave the ShE and are driven by the currents in southward and westward directions. The velocities of the CE are weaker (10–15 cm/s). In the Cyprus–Syria Passage drifter tracks depict an anticyclonic pattern (speeds between 25 and 35 cm/s; diameter of ~90 km).

In late fall 2009 and winter 2009–2010, drifters deployed along the south Israeli coast follow an anticyclonic meander located at 33.5°–34.5°N and 33.8°–35°E (Fig. 11a; speeds of 25–30 cm/s; diameter of ~120 km), continue northward (Fig. 11b) and turn in the CC (Fig. 11c). The CE is located between 32°E and 33.5°E (Fig. 11a and b) with velocities larger than 20 cm/s in the northern and western limbs. During winter (Fig. 11c) the CE appears elongated in the east-west direction (32°–34°E; diameter of 200 km) with higher velocities in the northern and eastern branches (larger than 25 cm/s).

In spring 2010 (Fig. 12a) the drifter tracks follow an anticyclonic eddy (core located at 34°N and 33.5°E), which could be identified as the ShE (speeds of 20–35 cm/s; diameter of 100–120 km), and a cyclonic secondary lobe (eddy core located at 33.5°N and 34.5°E; speeds of 15–30 cm/s; diameter of ~80 km). South of these

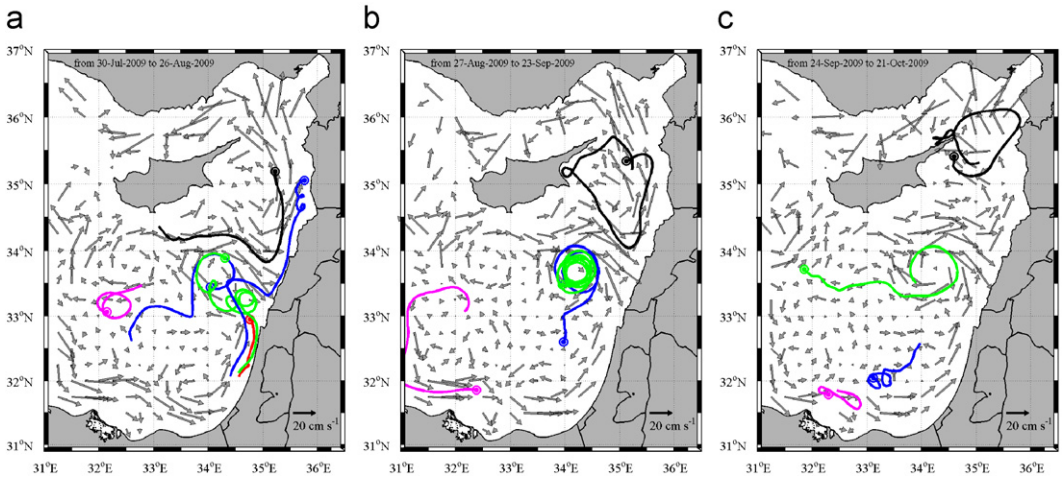

Fig. 10. Four-weekly mean unbiased geostrophic currents and NEMED drifter tracks (coloured lines) from 30-July-2009 to 26-August-2009 (a), from 27-August-2009 to 23-September-2009 (b), from 24-September-2009 to 21-October-2009 (c). Drifter ending points are shown with large circles.

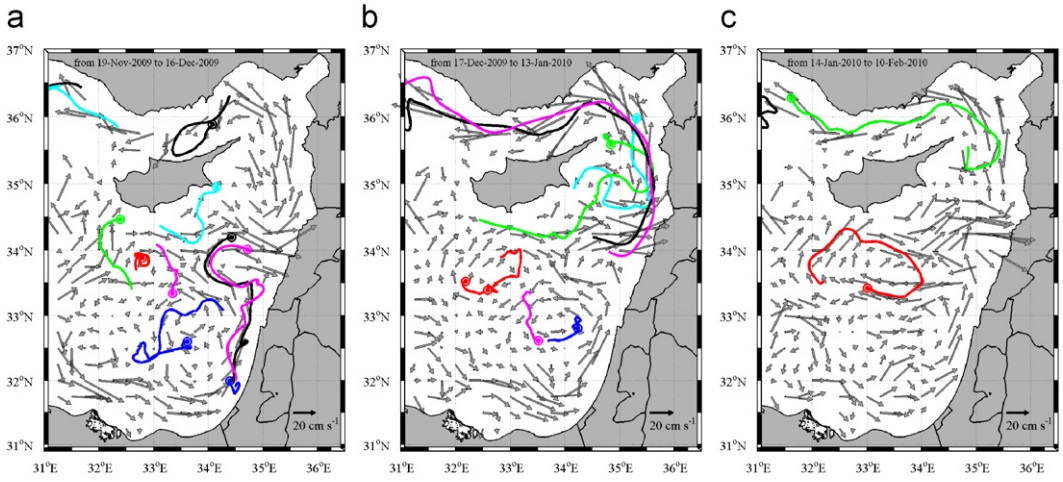

Fig. 11. Same as in Fig. 10 but from 19-November-2009 to 16-December-2009 (a), from 17-December-2009 to 13-January-2010 (b), from 14-January-2010 to 10-February-2010 (c).

structures there are two transient eddies: the western cyclonic eddy (core located at 32.35°N and 31.5°E) is characterised by velocities of 20 cm/s and a diameter of 100 km, while the eastern anticyclonic eddy (core located at 32.5°N and 34°E) is larger (diameter of ~150 km). The core of CE is located at 34°N and 31.6°E, with a diameter of ~120 km and velocities of 10–25 cm/s. The Latakia region is dominated by a cyclonic circulation with a diameter of ~50 km and speeds larger than 30 cm/s. During summer (Fig. 12b and c) the cyclonic secondary lobe becomes more intense (speeds larger than 35 cm/s in the northern branch). Drifter tracks follow the northward coastal current, with some anticyclonic recirculation, and finally turn into the CC. The Latakia region (Fig. 12c) shows an anticyclonic pattern (speeds between 15 cm/s and 30 cm/s; diameter of ~100 km).

In early fall 2010, the circulation is governed by a single anticyclonic eddy, mainly attributed to the CE, that occupies the region between 33°–34.5°N and 32.5°–35°E (Fig. 13a) with speeds larger than 25 cm/s. Southwest of the main eddy, drifter tracks depict a transient anticyclonic eddy located between 32°–33°N and 31.5°–32.3°E, and elongated in northwest–southeast directions with a zonal stretch of ~150 km. Late in fall, the main eddy reduces its diameter from 200 km (Fig. 13a) to 100 km (Fig. 13b and Fig. 13c) with speeds between 15 cm/s and 30 cm/s. The Latakia region shows a cyclonic circulation.

In summary, the monthly maps of the eastern LSB show: (1) the origin of the ShE as a pinched off meander from the costal current and confirms the variability and complexity of ShE generation area, characterised by transient cyclonic and anticyclonic eddies, as explained by Ayoub et al. (1998), Zodiatis et al. (1998) and Gertman et al. (2007); (2) the high variability in shape, size, location and intensity associated with the CE, in agreement with Groom et al. (2005) and Zodiatis et al. (2005); (3) the generation of LTE from the interaction of MMJ with the coastal current, as suggested by Zodiatis et al. (2003).

4. Summary and conclusions

The surface dynamic of the LSB derives from a complex and nonlinear interaction among multi-scale flow patterns. The basin circulation and the mesoscale and sub-basin scale eddies interact in a non-linear way, producing a high spatio-temporal variability of current field. This complex circulation cannot be simply characterised in terms of time-averages or of seasonal variability. Therefore, in this work we have described the patterns of geostrophic surface circulation in term of mean currents (1992–2010), seasonal changes and monthly temporal evolution (2009–2010), as derived from the analysis of drifter and satellite altimetry data.

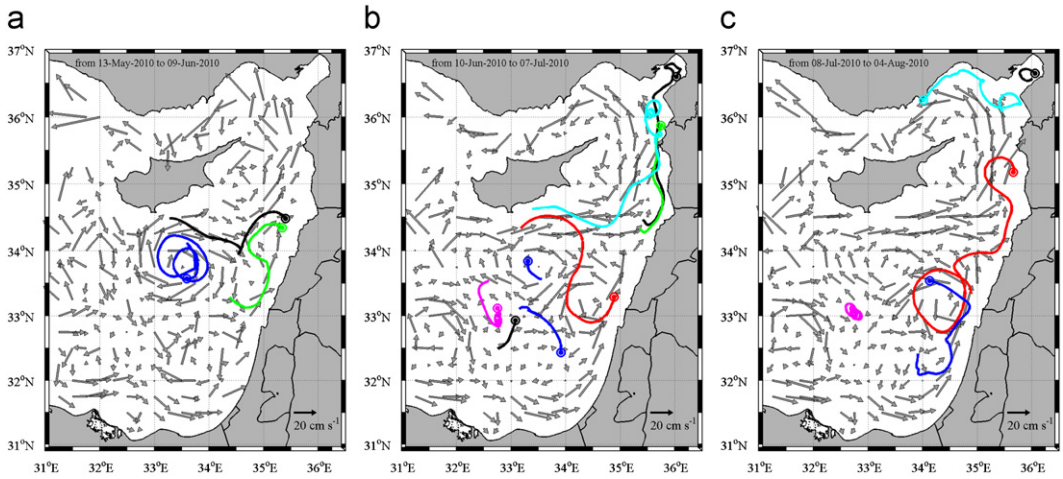

Fig. 12. Same as in Fig. 10 but from 13-May-2010 to 09-June-2010 (a), from 10-June-2010 to 07-July-2010 (b), from 08-July-2010 to 04-August-2010 (c).

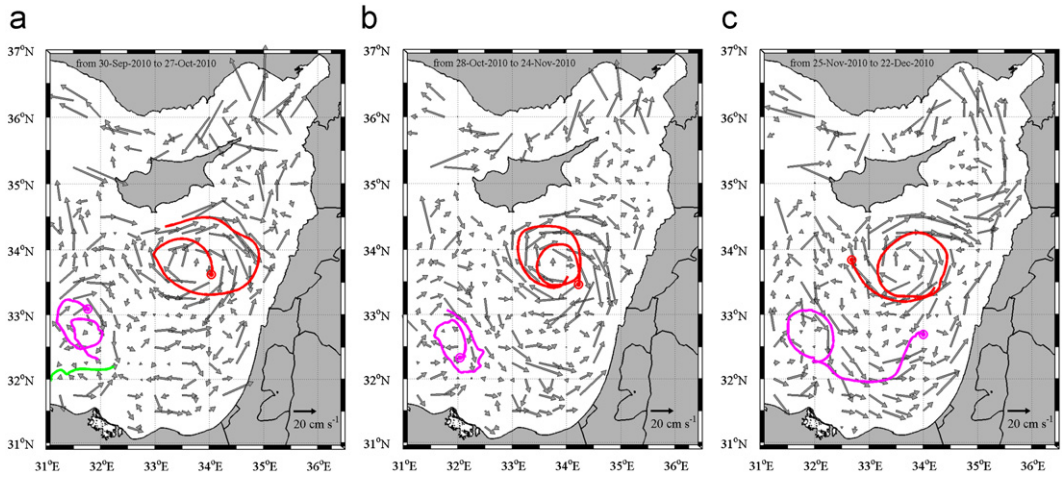

Fig. 13. Same as in Fig. 10 but from 30-September-2010 to 27-October-2010 (a), from 28-October-2010 to 24-November-2010 (b), from 25-November-2010 to 22-December-2010 (c).

Drifter and satellite altimeter data have been combined to construct a regularly sampled dataset of observations; the velocity statistics computed with this combined geostrophic currents are less affected by the non-uniform drifter sampling and then they are defined as 'unbiased'. The unbiased pseudo-Eulerian mean velocity field (Fig. 5a) depicts a cyclonic coastal circulation around the whole basin (LEC, CC, AMC) and an eastward zonal meandering flow (MMJ) in the central LSB. The along-slope current is characterised by mean speed of 15–20 cm/s along the Egypt–Israel–Lebanon coasts and of 25 cm/s in the Cyprus–Syria Passage and in the Cilician and Antalya sub-basins. The offshore current reaches intensities of 15–20 cm/s. The southern and eastern limbs of the along-slope current generate several sub-basin features such as the EE (speeds of 10–15 cm/s) and the ShE (speeds of 15–20 cm/s). The LTE (speed of ~10 cm/s) is generated by the interaction between the MMJ meandering and by the instability of the northward along-slope current. Two permanent anticyclonic eddies dominate the circulation of the western LSB: the IE, that reaches mean speed of 30 cm/s (MKE values of 250–300 cm^2/s^2; EKE larger than 600 cm^2/s^2), and the MME with mean speeds larger than 20 cm/s (MKE larger than 300 cm^2/s^2; EKE less than 100 cm^2/s^2). Southwest of Cyprus the anticyclonic CE is characterised by an intense northern limb (speed of 15–20 cm/s).

The unbiased geostrophic velocities (Fig. 5a) have been compared with the satellite absolute geostrophic velocities $\boldsymbol{U_{AGV}}$ (Fig. 5b) derived from the ADT (Rio et al. 2007). The comparison reveals salient differences both in terms of mean values and spatial structures. The currents $\boldsymbol{U_{AGV}}$ are more intense along the Egyptian slope and less intense along the Syrian and Turkish slope, while the diameters of IE and MME appear to be reduced by about 25 km. The $\boldsymbol{U_{AGV}}$ currents show a southward fast meander (speeds of 20–25 cm/s) between IE and MME (27°–28°E), identified as a part of the meandering MMJ (Rio et al., 2007; Amitai et al., 2010). This meander is not recognisable in the unbiased map but coincide with an area of high eddy variability (Fig. 6b, Fig. 7c and d). Moreover, the $\boldsymbol{U_{AGV}}$ map shows the inflow of surface waters in the LSB (at 25°E) through both the central MMJ and the along-slope current, whereas in the unbiased map the MMJ is located east of 28°E. The unbiased current field (Fig. 5a) is considered more realistic than the $\boldsymbol{U_{AGV}}$ (Fig. 5b) because it is based on a larger number of in-situ drifter observations in the LSB.

The unbiased map of MKE (Fig. 6a) shows larger values along the northern border of IE and MME, in agreement with the previous maps derived from the drifter data (Mauerhan, 2000; Gerin et al., 2009; Poulain et al., 2012) and from drifter/altimeter data (Poulain et al., 2012). In the region between IE and MME the unbiased EKE

levels (Fig. 6b) are comparable with the estimates of Mauerhan (2000) whereas, elsewhere they are 2–4 times smaller than those estimated directly from the drifter data (Mauerhan, 2000; Poulain et al., 2012). This discrepancy is mainly due to the possible residual wind-driven and non-geostrophic currents measured by the drifters and to the spatial smoothing applied to the satellite altimeter data (100 km scale, see Pujol and Larnicol, 2005).

Seasonal pseudo-Eulerian maps (Fig. 7) show higher speeds and energy levels in the extended summer than the extended winter, in particular in the IE and in the Latakia region.

The evolution of the kinetic energy of velocity residuals reveals an interannual spatio-temporal variability of eddies in the eastern LSB. The ShE has a periodic nature with higher intensities during fall and winter; its most intense activity is observed in the period 1998–2005. The CE has a less periodic nature, characterised by events of high KE and periods in which it extends eastward forming a large anticyclonic structure with a diameter of 250–300 km (Fig. 8c). The LTE is mainly cyclonic with higher values of KE in summer and fall. Occasional inversions of the circulation from cyclonic to anticyclonic (Fig. 9 and 12c), are induced by the interaction of MMJ with the northward meandering coastal current. The anticyclonic path persists for long periods between 2001 and 2006.

The monthly temporal evolution of sub-basin eddies in the eastern LSB confirm the high variability in shape and size of the CE and ShE, sometimes related to the occurrence of transient cyclonic and anticyclonic eddies. The variability of the LTE depends on the intensity of the MMJ and on the meandering nature of the along-slope northward current.

The combination of drifter and satellite data improves the quality of the description of the Mediterranean Sea surface circulation, because it allows to remove the biases that arise from the irregular sampling of drifters and to enhance the accuracy of satellite data in the coastal areas. In particular, the combined dataset provides a thorough description of the surface circulation in the LSB and underlines its improvement with respect to the satellite absolute geostrophic velocities obtained using previous methods (e.g. Rio et al., 2007). Moreover, the combined dataset gives a novel description of the sub-basin eddies in the eastern Levantine and emphasises their seasonal and interannual variations.

Acknowledgements

The authors would like to thank all the people who helped with drifter deployments, in particular technicians from Cyprus and Israel, and P. Testor and F. D'Ortensio for the deployments during the Tara expedition. The altimeter products were produced by Ssalto/Duacs and distributed by AVISO, with support from CNES. The NEMED project was supported by the Office of Naval Research under grants N000140810945. This work was also partially supported by Agenzia Spaziale Italiana as part of GOCE-Italy project. We thank the anonymous reviewers for their constructive comments.

Appendix A. Supplementary material

Supplementary data associated with this article can be found in the online version at doi:10.1016/j.dsr.2012.02.008.

References

Alhammoud, B., Branger, K., Mortier, L., Crepon, M., Dekeyser, I., 2005. Surface circulation of the Levantine basin: comparison of model results with observation. Prog. Oceanogr. 66, 299–320.

Amitai, I., Lehahn, Y., Lazar, A., Heifetz, E., 2010. Surface circulation of the eastern Mediterranean Levantine basin: insights from analyzing 14 years of satellite altimetry data. J. Geophys. Res. 115, C10058.

Atlas, R., Ardizzone, J.V., Hoffman, R., Jusem, J.C., Leidner, S.M., 2009. Cross-calibrated, multi-platform ocean surface wind velocity product (MEaSUREs Project). Guide Document. Physical Oceanography Distributed Active Archive Center (PO.DAAC). JPL, Pasadena, California, Version 1.0., 26p.

Ayoub, N., Le Traon, P.Y., De Mey, P., 1998. A description of Mediterranean surface variable circulation from combined ERS-1 and TOPEX/POSEIDON altimetric data. J. Mar. Syst. 18, 3–40.

Brenner, S., 1989. Structure and evolution of warm core eddies in the eastern Mediterranean Levantine basin. J. Geophys. Res. 94 (C9), 12593–12602.

Carval, T., Keeley, B., Takatsuki, Y., Yoshida, T., Loch, S., Schmid, C., Goldsmith, R., Wong, A., McCreadie, R., Thresher, A., Tran, A., 2008. Argos User's Manual.

Centurioni, L.R., Ohlmann, J.C., Niiler, P.P., 2008. Permanent meanders in the California current system. J. Phys. Oceanogr. 38, 1690–1710.

Centurioni, L.R., Niiler, P.N., Lee, D.-K., 2009. Near surface circulation in the South China Sea during the winter monsoon. Geophys. Res. Lett. 36, L06605.

Demirov, E., Pinardi, N., Fratianni, C., Tonani, M., Giacomelli, L., De Mey, P., 2003. Assimilation scheme of the Mediterranean forecasting system: operational implementation. Ann. Geophys. 21, 189–204.

Fusco, G., Manzella, G.M.R., Cruzado, A., Gacic, M., Gasparini, G.P., Kovacevic, V., Millot, C., Tziavos, C., Velasquez, Z.R., Walne, A., Zervakis, V., Zodiatis, G., 2003. Variability of mesoscale features in the Mediterranean Sea from XBT data analysis. Ann. Geophys. 21, 21–32.

Gaines, F., Copeland, M., Coban-Yildiz, Y., Ozsoy, E., Davie, A.M., Konovalov, S.K., 2006. The contrasting oceanography of the Rhodes Gyre and the Central Black Sea. Turkish J. Eng. Environ. Sci. 30, 69–81.

Gerin, R., Poulain, P.-M., Taupier-Letage, I., Millot, C., Ben Ismail, S., Sammari, C., 2009. Surface circulation in the Eastern Mediterranean using Lagrangian drifters (2005–2007). Ocean Sci. 5, 559–574.

Gertman, I., Zodiatis, G., Murashkovsky, A., Hayes, D., Brenner, S., 2007. Determination of the locations of southeastern Levantine anticyclonic eddies from CTD data. Rapp. Commun. Int. Mer. Mediterr. 38, 151.

Gertman, I., Goldman, R., Rosentraub, Z., Ozer, T., Zodiatis, G., Hayes, D., Poulain, P.-M., 2010. Generation Shikmona anticyclonic eddy from long shore current. Rapp. Commun. Int. Mer. Mediterr 39, 114.

Groom, S., Herut, B., Brenner, S., Zodiatis, G., Psarra, S., Kress, N., Krom, M.D., Law, C.S., Drakopoulos, P., 2005. Satellite-derived spatial and temporal biological variability in the Cyprus Eddy. Deep-Sea Res. 52, 2990–3010.

Group, P.O.E.M., 1992. General circulation of the Eastern Mediterranean. Earth Sci. Rev. 32, 285–309.

Hamad, N., Millot, C., Taupier-Letage, I., 2005. A new hypothesis about the surface circulation in the eastern basin of the Mediterranean Sea. Prog. Oceanogr. 66, 287–298.

Hamad, N., Millot, C., Taupier-Letage, I., 2006. The surface circulation in the eastern basin of Mediterranean Sea. Sci. Mar. 70 (3), 457–503.

Hansen, D.V., Poulain, P.-M., 1996. Processing of WOCE/TOGA drifter data. J. Atmos. Oceanic Technol. 13, 900–909.

Hayes, D., Testor, P., Zodiatis, G., Konnaris, G., Hannides, A., Mortier, L., Beguery, L., D'Ortenzio, F., Mauri, E., Lekien, F., Gerin, R., Poulain, P.-M., Lazar, A., 2010. Glider transects in the Levantine Sea: a study of the warm core Cyprus Eddy. Rapp. Commun. Int. Mer. Mediterr. 39, 116.

Hecht, A., Gertman, I., 2001. Physical features of the eastern Mediterranean resulting from the integration of POEM data with Russian Mediterranean Cruises. Deep-Sea Res. 48 (8), 1847–1876.

Hecht, A., Pinardi, N., Robinson, A.R., 1988. Current, water masses, eddies and jets in the Mediterranean Levantine basin. J. Phys. Oceanogr. 18, 1320–1353.

Kundu, P.K., 1976. Ekman veering observed near the ocean bottom. J. Phys. Oceanogr. 6, 238–242.

Larnicol, G., Ayoub, N., Le Traon, P.-Y., 2002. Major changes in Mediterranean Sea level variability from 7 years of TOPEX/POSEIDON and ERS-1/2 data. J. Mar. Syst. 33-34, 63–89.

Lascaratos, A., Roether, W., Nittis, K., Klein, B., 1999. Recent changes in deep water formation and spreading in the eastern Mediterranean Sea: a review. Prog. Oceanogr. 44 (1-3), 5–36.

Lascaratos, A., Williams, R.G., Tragou, E., 1993. A Mixed-layer study of the formation of levantine intermediate water. J. Geophys. Res. 98, 739–749.

Lumpkin, R., Pazos, M., 2007. Measuring surface currents with SVP drifters: the instrument, its data and some results. In: Griffa, A., et al. (Eds.), Lagrangian Analysis and Prediction of Coastal and Ocean Dynamics. Cambridge University Press, pp. 39–67.

Malanotte-Rizzoli, P., Bergamasco, A., 1991. The wind and thermally driver circulation of the eastern Mediterranean Sea. Part II: the baroclinic case. Dyn. Atm. Oceans 15 (3-5), 355–419.

Malanotte-Rizzoli, P., Manca, B., Ribera D'Alcala, M., Theocharis, A., Bergamasco, A., Bregant, D., Budillon, G., Civitarese, G., Georgopoulos, D., Michelato, A., Sansone, E., Scarazzato, P., Souvermezoglou, E., 1997. A synthesis of the Ionian Sea hydrography, circulation and water masses pathway during POEM-Phase I. Prog. Oceanogr. 39, 153–204.

Malanotte-Rizzoli, P., Robinson, A.R., 1988. POEM: Physical oceanography of the Eastern Mediterranean. EOS The Oceanogr. Rep 69 (14), 194–203.

Manzella, G.M.R., Cardin, V., Cruzado, A., Fusco, G., Gacic, G., Galli, C., Gasparini, G.-P., Gervais, T., Kovacevich, V., Millot, C., Petit De la Villeon, L., Spaggiari, G., Tonani, M., Tziavos, C., Velásquez, Z., Walne, A., Zervakis, V., Zodiatis, G., 2001.

EU-sponsored effort improves monitoring of circulation variability in the Mediterranen. EOS. Trans. AUG 82 (43), 497–504.
Mauerhan, T.A., 2000: Drifter Observations of the Mediterranean Sea Surface Circulation. Master of Science in Physical Oceanography. Thesis, Naval Postgraduate School, Monterey, CA, 111 pp.
Menna, M., Mauri, E., Poulain, P.-M., 2010. Correnti indotte dal vento e correnti geostrofiche nel Mar Mediterraneo. Rel. 2010/98 OGA 20 SIRE. OGS, Trieste, Italy. 73 pp.
Millot, C., 1999. Circulation in the Western Mediterranean Sea. J. Marine Syst. 20 (1-4), 423–442.
Millot, C., Gerin, R., 2010. The Mid-Mediterranean Jet Artefact. Geophys. Res. Lett. 37, L12602.
Millot, C., Taupier-Letage, I., 2005. Circulation in the Mediterranean Sea. Handb. Environ. Chem. 5 (K), 29–66.
Nielsen, J.N., 1912. Hydrography of the Mediterranean and adjacent waters. Rep. Dan. Ocean. Exp. Mediterr. 1, 77–192.
Niiler, P.P., Maximenko, N.A., Panteleev, G.G., Yamagata, T., Olson, D.B., 2003. Near-surface dynamical structure of the Kuroshio Extension. J. Geophys. Res. Oceans **108** (**C6**), 24–31. doi:10.1029/2002JC001461.
Ovchinnikov, I.M., 1966. Circulation in the surface and intermediate layer of the Mediterranean. Oceanol 6, 48–59.
Ovchinnikov, I.M., Plakhin, E.A., Moskalenko, L.V., Negliad, K.V., Osadchii, A.S., Fedoseev, A.F., Krivoscheya, V.G., Voitova, K.V., 1976. Hydrology of the Mediterranean Sea. Gidrometeoizdat, Leningrad (URSS), 375.
Özsoy, E., Hecht, A., Ünlüata, Ü., Brenner, S., Oguz, T., Bishop, J., Latif, M.A., Rozentraub, Z., 1991. A review of Levantine Basin circulation and variability during 1985–1988. Dyn. Atmos. Oceans 15, 421–456.
Özsoy, E., Hecht, A., Ünlüata, Ü., Brenner, S., Sur, H.I., Bishop, J., Latif, M.A., Rozentraub, Z., Oguz, T., 1993. A synthesis of the Levantine Basin circulation and hydrography, 1985–1990. Deep-Sea Res. 40, 1075–1119.
Ozsoy, E., Hecht, A., Unluata, U., 1989. Circulation and hydrography of the Levantine basin. Results of POEM coordinated experiments 1985–1986. Prog. Oceanogr. 22, 125–170.
Pascual, A., Pujol, M., Larnicol, G., Le Traon, P.Y., Rio, M., 2007. Mesoscale mapping capabilities of multisatellite altimeter missions: first results with real data in the Mediterranean Sea. J. Mar. Syst. 65 (1–4), 190–211.
Pinardi, N., Bonazzi, A., Dobricic, S., Milliff, R.F., Wikle, C.K., Berliner, L.M., 2011. Ocean ensemble forecasting. Part II: Mediterranean forecast system response. Q. J. R. Meteorol. Soc. 137, 879–893.
Pinardi, N., Masetti, E., 2000. Variability of the large-scale general circulation of the Mediterranean Sea from observations and modelling: a review. Palaeogeogr. Palaeoclimatol. Palaeoecol. 158 (21), 153–173.
Pinardi, N., Zavatarelli, M., Arneri, E., Crise, A., Ravaioli, M., 2006. The physical, sedimentary and ecological structure and variability of shelf areas in the Mediterranean Sea. In: Robinson, A.R., Brink, K. (Eds.), The Sea, vol. 14. Harvard University Press, Cambridge, USA, pp. 1245–1330.
Poulain, P.-M., 2001. Adriatic Sea surface circulation as derived from drifter data between 1990 and 1999. J. Mar. Syst. 29, 3–32.
Poulain, P.-M., Barbanti, R., Cecco, R., Fayes, C., Mauri, E., Ursella, L., Zanasca, P., 2004. Mediterranean surface drifter database: 2 June 1986 to 11 November 1999. Rel. 75/2004/OGA/31, OGS, Trieste, Italy (CDRom).
Poulain, P.-M., Gerin, R., Mauri, E., Pennel, R., 2009. Wind effects on drogued and undrogued drifters in the eastern Mediterranean. J. Atmos. Ocean Technol. 26, 1144–1156.
Poulain, P.-M., Menna, M., Mauri, E. Surface geostrophic circulation of the Mediterranean Sea derived from drifter and satellite altimeter data. J. Phys. Oceanogr., doi:10.1175/JPO-D-11-0159.1, in press.
Pujol, M.-I., Larnicol, G., 2005. Mediterranean Sea eddy kinetic energy variability from 11 years of altimetric data. J. Mar. Syst. 58 (3-4), 121–142.
Rio, M.-H., Hernandez, F., 2004. A mean dynamic topography computed over the world ocean from altimetry, in-situ measurements, and a geoid model. J. Geophys. Res. 109, C12032. doi:10.1029/2003JC002226.
Rio, M.-H., Poulain, P.-M., Pascual, A., Mauri, E., Larnicol, G., Santoleri, R., 2007. A mean dynamic topography of the Mediterranean Sea computed from altimetric data, in-situ measurements and a general circulation model. J. Mar. Syst. 65, 484–508.
Robinson, A.R., Golnaraghi, M., Leslie, W.G., Artegiani, A., Hecht, A., Lazzoni, E., Michelato, A., Sansone, E., Theocharis, A., Unluata, U., 1991. The eastern Mediterranean general circulation: features, structure and variability. Dyn. Atmos. Oceans 15, 215–240.
Robinson, A.R., Golnaraghi, M., 1993. Circulation and dynamics of eastern Mediterranean Sea; quasi-Synoptic data-driven simulation. Deep-Sea Res. 40 (6), 1207–1246.
Robinson, A.R., Hetch, A., Pinardi, N., Bishop, J., Leslie, W., Rosentroub, Z., Mariano, A., Brenner, S., 1987. Small synoptic/mesoscale eddies and energetic variability of the eastern Levantine basin. Nature 327, 131–134.
Robinson, A.R., Leslie, W.G., Theocharis., A., Lascaratos, A., 2001. Mediterranean Sea circulation. Encycl. Ocean Sci., 1689–1706.
Roussenov, V., Stanev, E., Artale, V., Pinardi, N., 1995. A seasonal model of the Mediterranean Sea general circulation. J. Geophys. Res. 100 (C7), 13515–13538.
Tziperman, E., Malanotte-Rizzoli, P., 1991. The climatological seasonal circulation of the Mediterranean Sea. J. Mar. Res. 49, 411–434.
Zodiatis, G., Drakopoulos, P., Brenner, S., Groom, S., 2005. Variability of Cyprus warm core eddy during the CYCLOPS project. Deep-Sea Res. 52, 2897–2910.
Zodiatis, G., Lardner, R., Lascaratos, A., Georgiou, G., Korres, G., Syrimis, M., 2003. High resolution nested model for Cyprus, NE Levantine basin, eastern Mediterranean Sea: implementation and climatological runs. Ann. Geophys. 21, 221–236.
Zodiatis, G., Hayes, D., Gertman, I., Samuel-Rhoads, Y., 2010. The Cyprus warm eddy and the Atlantic water during the CYBO cruises (1995–2009). Rapp. Commun. Mer Mediterr. 39, 202.
Zodiatis, G., Theodorou, A., Demetropulos, A., 1998. Hydrography and circulation south of Cyprus in late summer 1995 and in spring 1996. Oceanol. Acta 21, 447–458.